INTERNATIONAL JOURNAL FOR NUMERICAL METHODS IN FLUIDS, VOL. 22, 495–513 (1996)

A VORTEX LATTICE METHOD FOR HIGH-SPEED PLANING

CANHAI LAI AND ARMIN W. TROESCH

Department of Naval Architecture and Marine Engineering, The University of Michigan, Ann Arbor, MI 48109, U.S.A.

SUMMARY

A three-dimensional numerical model using vortex lattice methods (VLMs) is developed to solve the steady planing problem. Planing hydrodynamics have similarities to the aerodynamic swept wing problem—the fundamental difference being the existence of a free surface. Details of the solution scheme are discussed, including the special features of the VLM used here in obtaining accurate flows at the leading and side edges. Computational results are presented and compared with existing theories and experiments.

KEY WORDS: hydrodynamic planing; vortex lattice; jet modelling

INTRODUCTION

Vortex lattice methods (VLMs) have an extensive history, one primarily associated with lifting wings in aerodynamics. During the period 1911–1918, Prandtl[1] introduced the concept of the lifting line theory for a high-aspect-ratio wing. Based upon that work, a lifting surface theory which represents the flow by a surface vorticity distribution has evolved. The vortex lattice method results when the vorticity distribution is discretized in three dimensions. Since then the VLM has often been applied in the calculation of lift on wings, including delta wings.

One characteristic of a delta wing is flow separation along its leading edges. Various numerical methods employing the VLM have been used to study leading edge vortex separation, principally through the generation of free vorticity (see e.g. Reference 2).

Free vorticity has also been studied extensively in the treatment of the wake. Different methods are available, some of which can simulate wake roll-up accurately modelling the actual phenomenon. For the overall pressure distribution on the lifting surface, however, the accuracy of the treatment of the wake is important only at the trailing edge.[3]

Higher-order boundary element methods are often used to obtain improved accuracy. As for a non-lifting body where a continuous surface source distribution is more accurate than a discrete source distribution, a lifting body with a surface vorticity distribution brings more accurate results than the conventional vortex lattice method. Mracek and Mook,[4] for example, used a surface vorticity distribution and γ_x and γ_y in each panel as unknowns, where additional equations came from the constraint that the divergence of the curl of a vector field is always zero. This method, however, requires extra computational effort. For lifting wing problems, where the pressure difference between two sides rather than the absolute pressure itself is the desired quantity, this approach has not gained much popularity.

Wagner,[5] in analysing hydrodynamic planing, discovered that the flow beneath the planing hull surface is exactly the same as the flow on the lifting side of a wing except at the leading edge. Two-

CCC 0271–2091/96/010495-19

Received 5 May 1994
Revised 5 May 1995

dimensional theories for planing problems were developed following almost the same path as that in aerodynamics. Wagner[5] and Green[6] both used hodograph methods for their two-dimensional problem approximating the high-aspect-ratio three-dimensional planing hull. Tulin[7] used two-dimensional vortex distributions for his slender body planing hull model. Zhao and Faltinsen[8] and Vorus[9,10] used two-dimensional vortex distributions for their two-dimensional impact problems which can be related to slender body planing hulls under careful co-ordinate transformation and interpretation. Ogilvie[11] and Olgivie and Shen[12] also used vortex distributions to describe the unsteady two-dimensional flow for a high-aspect-ratio planing hull. At the leading and side edges (wetted hull chines), instead of the separation of the flow, there is a free surface which becomes the kernel of the planing problem.

Lai and Troesch[13] have discussed and developed modelling issues associated with planing such as slenderness, linearity of boundary conditions, wetted surface contours, jet development and panel shape. Results were compared with existing theories and experiments. In this paper, numerical details of the vortex lattice method used by Lai and Troesch[13] are presented.

AN OVERVIEW OF THE CURRENT MODEL

The previous section has identified several features of lifting wings and the vortex lattice method: leading edge separation, the wake vortex and high-order methods useful in detailing local behaviour. For the planing problem there are additional aspects that must be resolved before a successful computational model can be developed: a free surface outside the leading and side edges and continuity of velocity along all edges. It follows then that special modifications are needed for the traditional VLM to be applied in the planing problem. Briefly, the major modifications are described below.

1. At the leading and side edges of the planing hull the flow is modelled by a jet region where a non-linear dynamic free surface condition (the zero-pressure condition) is applied and the details of the actual jet spray are neglected. In the chines wet region (i,.e. the flow regime near the side) the Euler equation is used to determine the velocity field on the free surface. In this paper, emphasis is placed upon the numerical treatment of these leading and side edge jets, where a strong singularity occurs and a special vortex method is introduced. Unlike the wing problem where the main concern is the pressure difference between the suction side and the pressure side, the planing problem lacks a suction side. This increases the sensitivity of the planing lift calculation to changes in the edge modelling. Therefore the accuracy of the leading and side edge vorticity distributions (and resultant locally large pressures) becomes of paramount concern.
2. The existence of a jet region and a continuity condition on the vorticity distribution between the leading and side edges and the jet region removes the edge singularity. Conventional vortex lattice methods do not provide a continuous and therefore accurate vorticity distribution. In this work the VLM is a higher-order vortex lattice with a linear variation in strength. An accurate leading and side edge behaviour is thus obtained and hence the continuity condition and the zero-pressure condition are implemented.
3. Unlike the well-developed wing problems where sophisticated wake models such as 'wake relaxation' and the 'time-stepping method'[14] are derived when details of the trailing edge are needed, a so-called 'prescribed wake shape' model is used in the current VLM model. Similarly to the wake treatment in wing problems as indicated by Hoeijmakers,[3] this simplified downstream wake model yields satisfactory pressure distributions on the lifting side of the body.

PROBLEMS DEFINITION

As shown by Lai and Troesch,[13] a steady three-dimensional planing problem is formulated in terms of a velocity potential which is then solved by either the $z=0$ model (both vortex lattices and control points where the boundary conditions are satisfied are on the $z=0$ plane) or the $z=h$ model (both vortex lattices and control points are on the exact body). The co-ordinate system is depicted in Figure 1. The chines wet area is defined as the area where the hard chine is wet (with length L_c), i.e. $L_k - L_c \leqslant x \leqslant L_k$; in front of that is the chines dry part, i.e. $0 \leqslant x \leqslant L_x - L_c$. In this work the expression *leading edge* refers to the water–air–hull contact line in the chines dry area and the expression *side edge* refers to the water–air–hull contact line in the chines wet area. The flow is fundamentally different in these two areas, as shown schematically in Figure 1(b). The angle between the keel and the spray line is defined as the apex angle θ. There are a number of sources to determine the wetted surface (the value of θ); see the discussion in Reference 13. The result from Vorus's[9,10] analysis of the impact problem is applied in the present calculation. His method has the advantage over traditional empirical formulaes of including variable dead-rise effects.

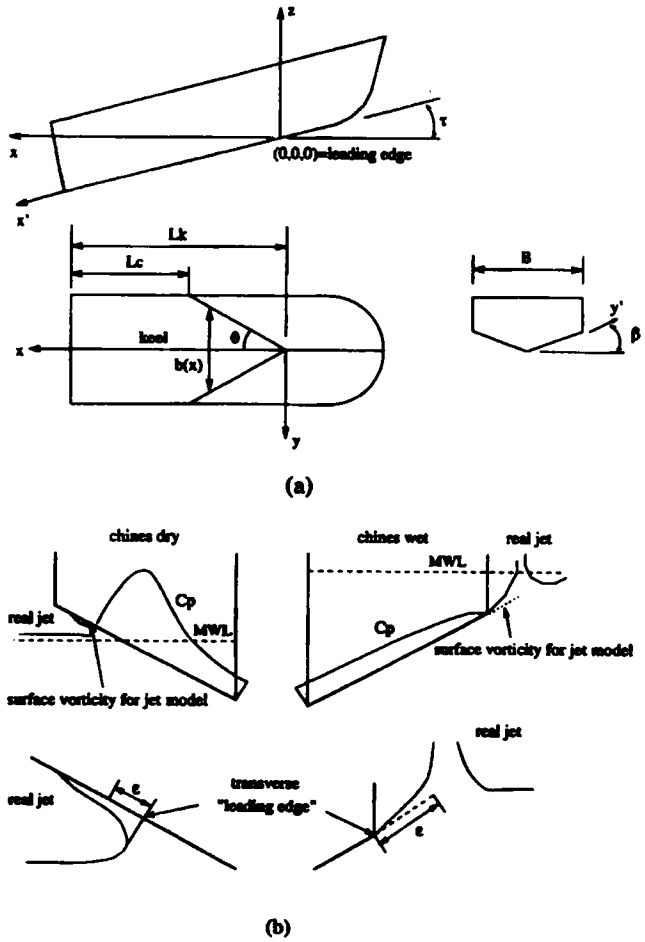

Figure 1. (a) Co-ordinate system definition; (x, y, z) is for $z=0$ model, while x' and y' are local co-ordinates defined for $z=h$ model. (b) Jet location and modelling details for both chines dry ($0 \leqslant x \leqslant L_k - L_c$) and wet ($L_k - L_c < x \leqslant L_k$) parts for $z=h$ model, where MWL indicates mean water line

The following defines the boundary value problem.

Velocity potential

$$\Phi = Ux + \phi, \tag{1}$$

where U is the uniform stream velocity and ϕ is the perturbation potential. Both Φ and ϕ satisfy Laplace's equation.

Body boundary condition

$$\frac{\partial \phi}{\partial z} - \left(U + \frac{\partial \phi}{\partial x}\right)\frac{\partial h}{\partial x} - \frac{\partial \phi}{\partial y}\frac{\partial h}{\partial y} = 0 \quad \text{on } z = 0 \tag{2}$$

for the $z = 0$ model and

$$\frac{\partial \phi}{\partial z} - \left(U + \frac{\partial \phi}{\partial x}\right)\frac{\partial h}{\partial x} - \frac{\partial \phi}{\partial y}\frac{\partial h}{\partial y} = 0 \quad \text{on } z = h(x, y) \tag{3}$$

for the $z = h$ model, or written in normal components,

$$\frac{\partial \Phi}{\partial n} = U \cdot n_x + \frac{\partial \phi}{\partial n} = 0 \quad \text{on } z = h(x, y), \tag{4}$$

where $\vec{n} = (n_x, n_y, n_z)$ is the unit normal fo the surface $z = h(x, y)$.

Free surface boundary condition

For the far field the free surface boundary condition is reduced to a zero-potential condition. For the near field it represents a zero-pressure condition:

$$U\frac{\partial \phi}{\partial x} + \frac{1}{2}\left(\frac{\partial \phi}{\partial x}\right)^2 + \frac{1}{2}\left(\frac{\partial \phi}{\partial y}\right)^2 = 0 \quad \text{on } z = 0 \tag{5}$$

for the $z = 0$ model and

$$U\frac{\partial \phi}{\partial x} + \frac{1}{2}\left(\frac{\partial \phi}{\partial x}\right)^2 + \frac{1}{2}\left(\frac{\partial \phi}{\partial y}\right)^2 + \frac{1}{2}\left(\frac{\partial \phi}{\partial z}\right)^2 = 0 \quad \text{on } z = \eta \tag{6}$$

for the $z = h$ model, or with gravity effects,

$$gz + U\frac{\partial \phi}{\partial x} + \frac{1}{2}\left(\frac{\partial \phi}{\partial x}\right)^2 + \frac{1}{2}\left(\frac{\partial \phi}{\partial y}\right)^2 + \frac{1}{2}\left(\frac{\partial \phi}{\partial z}\right)^2 = 0 \quad \text{on } z = \eta. \tag{7}$$

Velocity continuity on the chine

This condition requires the flow to leave the chine edge smoothly, i.e.

$$\vec{V} \neq \infty \tag{8}$$

at $y = \pm b(x)/2$ for $0 \leqslant x \leqslant L_k$.

Kutta condition for the trailing edge

The flow is required to leave the trailing edge smoothly, i.e.

$$\frac{\partial \phi}{\partial x} = 0 \quad \text{at } x = L_k. \tag{9}$$

Radiation condition

There is no perturbation velocity in the far field except in the area directly behind the trailing edge.

Pressure distribution

The pressure expression in terms of the velocity potential is

$$\frac{p}{\rho} = -U\frac{\phi}{\partial x} - \frac{1}{2}\left(\frac{\partial \phi}{\partial x}\right)^2 - \frac{1}{2}\left(\frac{\partial \phi}{\partial y}\right)^2 \tag{10}$$

for the $z = 0$ model and

$$\frac{p}{\rho} = -U\frac{\partial \phi}{\partial x} - \frac{1}{2}\left(\frac{\partial \phi}{\partial x}\right)^2 - \frac{1}{2}\left(\frac{\partial \phi}{\partial y}\right)^2 - \frac{1}{2}\left(\frac{\partial \phi}{\partial z}\right)^2 \tag{11}$$

for the $z = h$ model, or with gravity effects,

$$\frac{p}{\rho} = -gz - U\frac{\phi}{\partial x} - \frac{1}{2}\left(\frac{\partial \phi}{\partial x}\right)^2 - \frac{1}{2}\left(\frac{\partial \phi}{\partial y}\right)^2 - \frac{1}{2}\left(\frac{\partial \phi}{\partial z}\right)^2. \tag{12}$$

Here p is relative to atmospheric pressure. An integration of pressure over the body yields the lift force and trimming moment.

NUMERICAL METHOD

Before a vortex lattice method is applied, the model is formulated in terms of a vorticity distribution. In this section, details of the VLM are discussed, and the conversion from the vortex lattice distribution to a vorticity distribution is explained.

Surface vortex distribution

A surface vortex distribution $\gamma(x, y) = \gamma_x(x, y)\vec{i} + \gamma_y(x, y)\vec{j}$ is distributed on both the planning hull and the free surface. The perturbation velocity is

$$\nabla\phi(x, y, z) = \frac{1}{4\pi}\int\int_S \vec{\gamma}(\xi, \eta) \times \frac{(x-\xi)\vec{i} + (y-\eta)\vec{j} + z\vec{k}}{[(x-\xi)^2 + (y-\eta)^2 + z^2]^{3/2}}\,\mathrm{d}\xi\,\mathrm{d}\eta, \tag{13}$$

or for the lower surface in the fluid domain

$$\nabla\phi(x, y, z) = -\frac{\gamma_y}{2}\vec{i} + \frac{\gamma_x}{2}\vec{j} + \frac{1}{4\pi}\int\int_{S'} \vec{\gamma}(\xi, \eta) \times \frac{(x-\xi)\vec{i} + (y-\eta)\vec{j} + z\vec{k}}{[(x-\xi)^2 + (y-\eta)^2 + z^2]^{3/2}}\,\mathrm{d}\xi\,\mathrm{d}\eta, \tag{14}$$

where x and y are two coordinates locally tangent to the surface. As shown in Figure 2, $S - S_B + S_\varepsilon + S_w + S_o$, S' is S excluding point (x, y, z), and S_B is the region of the lifting surface; S_ε is the region of the jet area; S_w is the region of the downstream area; and S_o is the region of the upstream area. S_ε is not known beforehand and must be determined through iteration.

For the $z = 0$ model the potentials for the planing hull surface and free surface are evaluated on the $z = 0$ plane and the above expression can be simplified:

$$\nabla\phi(x, y, 0) = -\frac{\gamma_y}{2}\vec{i} + \frac{\gamma_x}{2}\vec{j} + \frac{\vec{k}}{4\pi}\int\int_{S'} \frac{\gamma_x(y-\eta) - \gamma_y(x-\xi)}{[(x-\xi)^2 + (y-\eta)^2]^{3/2}}\,\mathrm{d}\xi\,\mathrm{d}\eta. \tag{15}$$

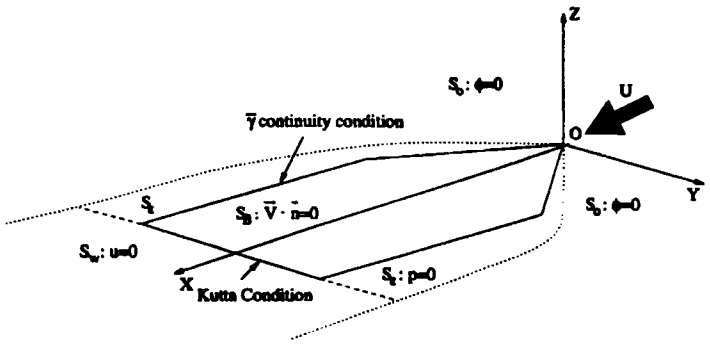

Figure 2. Schematic diagram of computational domain for $z=0$ model

Condition for potential flow

When the surface vorticity is distributed, the flow outside the surface is potential. However, from the fact that the divergence of the curl of a vector field is always zero, there is constraint equation for the vorticity distribution:

$$\nabla \cdot \vec{\gamma} = 0. \tag{16}$$

Body boundary condition

In S_B, the planing hull surface (for the $z=h$ model) or its projection on the $z=0$ surface (for the $z=0$ model), the body boundary condition must be satisfied. Substituting equation (14) into equation (2) yields

$$\frac{\partial h}{\partial x}\frac{\gamma_y}{2} - \frac{\partial h}{\partial y}\frac{\gamma_x}{2} + \frac{1}{4\pi}\iint_S \frac{\gamma_x(y-\eta)-\gamma_y(x-\xi)}{[(x-\xi)^2+(y-\eta)^2]^{3/2}}\,d\xi\,d\eta = U\frac{\partial h}{\partial x}, \tag{17}$$

where $(x, y) \in S_B$.

Free surface boundary condition

The entire free surface is divided into several regions where the free surface boundary conditions applied are different in form.

Downstream and far upstream the velocity potential can be expressed in terms of a dipole distribution as

$$\phi(x,y,z) = -\frac{z}{4\pi}\iint_S \frac{\mu(\xi,\eta)\,d\xi\,d\eta}{[(x-\xi)^2+(y-\eta)^2+z^2]^{3/2}}, \tag{18}$$

where μ is the dipole strength. (Vortex lattices are essentially the same as surface dipole distributions.) Distributing no vortex lattice in the area S_0 satisfies the zero-potential condition[13] for the $z=0$ model. For the $z=h$ model, vortex lattices are distributed on near-field surfaces, i.e. hull and jet; equation (18) shows that the potential behaves like $O(1/R^2)$ as $R \to \infty$, where R is the distance from the fat-field calm water surface to the vorticity surface in the near field. Therefore for the $z=h$ case the far-field zero-potential condition is satisfied asymptotically.

In the wake region S_w, $\partial\phi/\partial x = 0$. From equation (14), $\gamma_y = 0$ or

$$\nabla \cdot \vec{\gamma} = \frac{1}{2}\frac{\partial \gamma_x}{\partial x} = 0, \tag{19}$$

which implies

$$\gamma_x(x, y) = \gamma_x(y). \tag{20}$$

For the near-field free surface, in the jet region S_ε the near-field dynamic FSBC is applied:

$$U\frac{\partial \phi}{\partial x} + \frac{1}{2}\left(\frac{\partial \phi}{\partial x}\right)^2 + \frac{1}{2}\left(\frac{\partial \phi}{\partial y}\right)^2 = 0. \tag{21}$$

For the $z = 0^-$ the velocity can be expressed in terms of the $\vec{\gamma}$-distribution:

$$\nabla\phi = \left(\frac{\partial \phi}{\partial x}\right)\vec{i} + \left(\frac{\partial \phi}{\partial y}\right)\vec{j} + \left(\frac{\partial \phi}{\partial z}\right)\vec{k} \tag{22}$$

$$= \tfrac{1}{2}\gamma_x\vec{j} - \tfrac{1}{2}\gamma_y\vec{i} + w\vec{k}. \tag{23}$$

Substituting equation (23) into the dynamic FSBC (5) yields

$$\gamma_x^2 + \gamma_y^2 = 4U\gamma_y. \tag{24}$$

The jet thickness ε is developed as the flow passes the planing plate. There are two approaches to modelling the jet.

Approach 1: setting γ_x constant at each x-location

$$\gamma_x(x, y) = \gamma_x\left(x, \frac{b^+}{2}\right) \quad \text{for} \frac{b(x)}{2} < y \leqslant \frac{b(x)}{2} + \varepsilon(x). \tag{25}$$

Owing to symmetry, an analogous expression can be written for $y < 0$. Equation (25) implies that γ_x in the jet region is constant along the jet for each x but that γ_y may vary. Equation (24) is strictly valid only at $y = b^+/2$ and the pressure in the ε-area equals zero only approximately. This approximation neglects the convection of the jet vortex and is a literal interpretation of Tulin's[7] model.

This approach is suitable for the chines dry section but not for the chines wet section. In the chines dry section, $\vec{\gamma}$ remains a constant vector approximately within a small region ε; therefore, by fixing γ_x, γ_y is also determined and equation (24) is satisfied within the entire jet region. In the chines wet section, however, the jet thickness ε is relatively large, γ_y cannot be set to a constant by simply fixing γ_x and thus this approach is not appropriate.

Approach 2: computing γ_x along the jet region by the Euler equation. For our ideal flow the Euler Equation is

$$\frac{D\vec{V}}{Dt} = -\frac{1}{\rho}\nabla p + \frac{1}{\rho}\vec{F}. \tag{26}$$

There is no external force except gravity in the z-direction. Considering only the $z = 0$ plane, the requirement that the pressure in the jet area be constant yields

$$\frac{\partial p}{\partial x} = 0 \quad \rightsquigarrow \quad \frac{Du}{Dt} = 0, \tag{27}$$

$$\frac{\partial p}{\partial y} = 0 \quad \rightsquigarrow \quad \frac{Dv}{Dt} = 0. \tag{28}$$

If $p = 0$ at $y = b^+(x)/2$, we need only equation (28) to ensure that $p = 0$ in the entire ε-region.

At $z = 0^-$

$$\vec{V} = U\vec{i} + \nabla\phi = \left(U - \frac{\gamma_y}{2}\right)\vec{i} + \frac{\gamma_x}{2}\vec{j} + w\vec{k}. \tag{29}$$

Equation (28) is therefore equivalent to

$$\frac{D\gamma_x}{Dt} = 0 \tag{30}$$

or, if $\partial/\partial t = 0$ for steady flows,

$$(\vec{V} \cdot \nabla)\gamma_x = 0. \tag{31}$$

Equation (31) means that the γ_x-distribution along a streamline is constant. For the $z = 0$ model, $\vec{V}$ is considered only to have two tangential components and thus the streamline remains on the $z = 0$ plane. This approach is used only in the chines wet section. Vorus[9,10] derived a similar condition for his finite width wedge impact problem. The details of the implementation of this equation are shown in the next section. For the $z = h$ model, $\partial\phi/\partial y$ is due essentially to γ_x, so the above equation is also applicable.

Velocity continuity between the hull and the ε-area

This is a condition at the leading and side edges which is similar to the Kutta condition for the trailing edge. $\vec{V} < \infty$ requires

$$\vec{\gamma}\left(x, \frac{b^-}{2}\right) = \vec{\gamma}\left(x, \frac{b^+}{2}\right). \tag{32}$$

Because the potential in $y = S^+(x)/2$ is approximately constant, $\vec{\gamma}$ at the edge is approximately tangent to the edge.

Kutta condition at the trailing edge

One form of the Kutta condition requires

$$\frac{\partial\phi}{\partial x} = -\tfrac{1}{2}\gamma_y = 0 \quad \text{at the trailing edge,} \tag{33}$$

which means that the vortex leaves the trailing edge in the direction of the uniform stream. Therefore in the wake region S_w, $\vec{\gamma} = \gamma_x\vec{i}$.

Vortex lattice method

The boundary value problem now becomes one of obtaining a vorticity distribution in the computational surface which includes the body surface or its projection on the $z = 0$ plane and a jet immediately outside the chine. This jet region S_ε has unknown thickness and is determined through satisfying equations (16), (17), (20) and (24) with (25) or (31), (32) and (33). A surface vorticity distribution can be used to solve the BVP, where the unknowns are defined as the vorticity strengths γ_x and γ_y and the jet thickness ε. Using panel methods, there are two unknowns (γ_x and γ_y) in each panel and ε for each edge segment. Equation (16) provides additional conditions. The system can be solved iteratively (see e.g. Reference 4), but this requires extra computational effort. In addition, using a surface vortex distribution makes it difficult to accurately calculate the velocity potential. The vortex lattice method (VLM) is a generally used alternative, since Laplace's equation is automatically satisfied and the equivalence between the vortex lattice and the normal dipole distribution with constant strength provides a simple formula to obtain the velocity potential.[15] The vortex lattice method is used here with modifications necessary to provide the accurate detail at the edges.

Vortex lattices are distributed on the surface $z = 0$ or on the exact body depending upon the model used. The velocity integrated from S' can be obtained by using the Biot–Savart law. γ_x and γ_y are evaluated by averaging Γ over one panel and then u and v are simply expressed by equation (14). The Kutta condition (33) is satisfied by simply placing a vortex lattice away from the trailing edge, while the condition on the wake region, equation (20) is satisfied by placing horseshoe vortex lattices in the region. The remaining conditions that need to be satisfied are (17) and (24) with (25) or (31) and (32).

A description of the computer algorithm, including how $\vec{\gamma}$ is calculated from discrete vortex lattices, is given in the next section.

COMPUTER ALGORITHM

This section discusses details of panelization, $\vec{\gamma}$ calculation, jet thickness ε calculation, overall numerical iteration and computation steps. All the details are for the $z = 0$ model. The $z = h$ model, while more complicated, can be developed in a similar manner.

Panelization

Vortex lattice panels are distributed in the computational surface of the hull and the jet region. The body boundary conditions are satisfied at the control points which are located at the centroid of each panel. The zero-pressure condition is satisfied in the jet region from the edge $y = b(x)/2$ to the jet head $y = b(x)/2 + \varepsilon(x)$, where $b(x)$ is the local beam and $\varepsilon(x)$ is the local jet thickness.

In addition to the common characteristics of VLMs, three special features have been implemented in the current vortex lattice model: overlap panels which all start from the keel are used; subpanels with linear strength inside each regular panel are added; the vorticity strength in the x-direction, γ_x, for each panel is treated as an unknown.

Overlap vortex lattice. One difference between standard VLMs and the one developed here is the use of overlap vortex lattices: in each row, every panel begins at the same $y = 0$ keel location. The advantage of this is that it enables us to calculate γ_x more easily. If the planing hull is geometrically symmetrical, then for steady motion, or for unsteady motion without yaw, roll and sway, the $\vec{\gamma}$-distribution must be symmetrical as well:

$$\gamma_x(x, y) = -\gamma_x(x, -y), \qquad \gamma_y(x, y) = \gamma_y(x, -y). \tag{34}$$

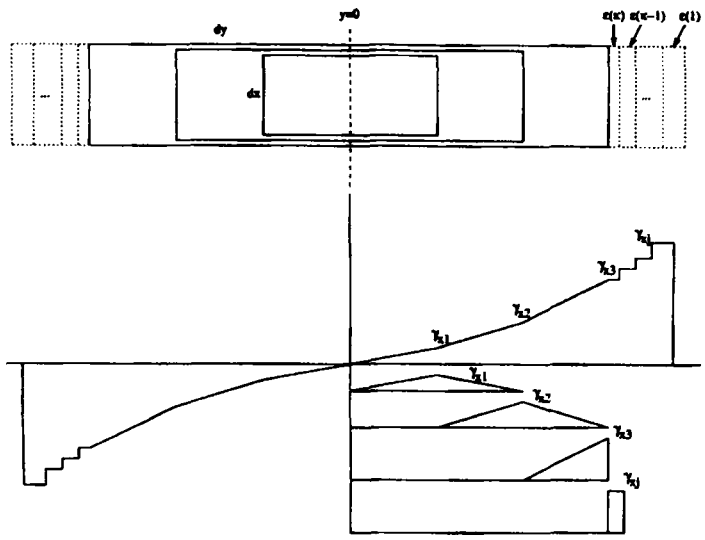

Figure 3. Local panelization for kth row

As shown in Figure 3, the vortex lattices from $y = -a$ to 0 and from $y = 0$ to a are combined to give one from $y = -a$ to a, thus reducing the number of unknown γ_x by a factor of two.

Subpanels for continuous γ_x-distribution. In order to obtain more accurate details of $\vec{\gamma}$ especially in panels near the chine, γ_x inside each panel is defined to vary linearly. For a non-rectangular panel where the integration of the vertical velocity induced by the vortex lattice is not easy, many subpanels are placed inside a vortex lattice to approximate a continuous γ_x-distribution. As mentioned previously, the use of cosine spacing can also help to accomplish this purpose. Figure 3 depicts the panelization in detail.

Vorticity strength γ_x as the unknown. The current vortex method defines the unknown as the vorticity strength in the x-direction, γ_x, instead of the circulation Γ. γ_x is piecewise linear inside each panel and the vortex lattice circulation strength of each subpanel is $\Gamma = \gamma_x \delta y$, where $n_s \delta y = \Delta y$ and Δy, δ and n_s are the width of the panel, the width of the subpanel and the number of subpanels inside a panel respectively. As shown in Figure 3, the linear variation in the γ_x-distribution on the body is achieved by tent functions with unknowns defined as the vorticity strength in the x-direction in the body, $\gamma_{xB}(i, j)$ $(i = 1, n_x; j = 1, n_y)$, while in the jet area the γ_x-distribution is piecewise constant and defined by a step function of unknowns $\gamma_{xJ}(i)$ $(i = 1, n_x)$, where n_x is the panel number in the x-direction and n_y in the y-direction

When $n_s = 1$, the current vortex model can be reduced to the conventional VLM. When $n_s = \infty$, it results in a piecewise continuous γ_x-distribution, while γ_y is still represented by discrete Γ and can be obtained in an averaging manner. The induced velocity at each control point by each subpanel is calculated using the Biot–Savart law and the results are summarized and redistributed to each unknown $\gamma_{xB}(i, j)$ and $\gamma_{xJ}(i)$. For a rectangular panel, $n_s = \infty$ is chosen and the summation is completed by an analytic integration. For a trapezoidal panel, owing to the difficulty of analytic integration, $n_s = 15$ is used for most the cases in this study. In this case, γ_x is still discrete.

The advantage of using higher-order subpanels is that the method gives more accurate details of γ_x-variation in the y-direction without requiring significant additional computing time. The details of the γ_x-distribution in the leading and side edges are of particular interest, since it affects the jet properties; unfortunately, γ_x changes rapidly there and cannot be obtained accurately by the general VLM with a moderate number of panels. It is not desirable to obtain higher accuracy by simply increasing the

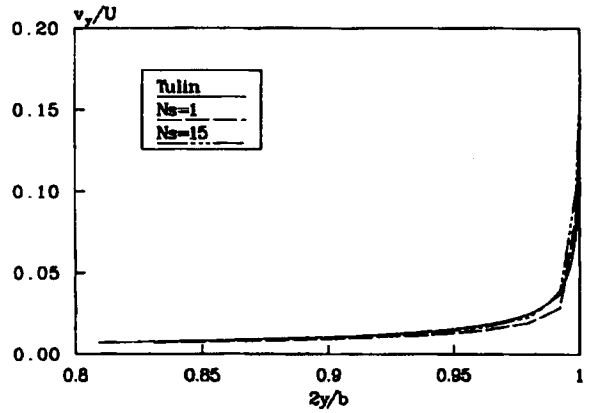

Figure 4. Calculation of transverse velocity for middle section ($x = 0{\cdot}5L_k$) at leading edge with and without subpanels. $\beta = 6°$, $\tau = 0{\cdot}3°$. Panel 2(20,0,20)

number of panels, since most of the required CPU is a result of the matrix solver in the iteration. Using subpanels provides a more economical alternative. As demonstrated in Figure 4, for a moderate panel number size, v_y with $n_s = 15$ is much closer to Tulin's[17] result than v_y with $n_s = 1$. The y-axis has an expanded scale to emphasize the differences.

ANALYSIS OF VARIOUS MODELLING DETAILS

This section focuses on details of the models mentioned in the main text. These include $\vec{\gamma}$ at the leading edge, $\vec{\gamma}$ in the jet region, the wake treatment, wetted surface contours and the convergence of the current numerical schemes. The numerical implementation of the γ_x and γ_y model generally follows Mook[16] and Thrasher;[17] detailed descriptions of the ε numerics, the matrix solver and the iteration scheme are given by Lai.[18]

$\vec{\gamma}$ at the leading edge

The $\vec{\gamma}$-distribution at the leading edge is finite, but it is very large compared with that in the rest of the planing hull surface and thus has a sharp ascent near the leading edge. Therefore, to obtain more precise details of $\vec{\gamma}$ in that region, the panelization has to be fine, with, ideally, cosine panel spacing. Other quantities such as the velocity and pressure distribution can be obtained fairly accurately by moderate panelization.

In lifting surface theory[14] the $\vec{\gamma}$-distribution at the leading edge is infinite and tangent to the edge. This can be explained as follows. First consider that the $\vec{\gamma}$-distribution outside the lifting surface is zero. By continuity, $\vec{\gamma} \cdot \vec{e}_n = 0$; therefore $\vec{\gamma} = \gamma_t \cdot \vec{e}_t$, i.e. $\vec{\gamma}$ is tangent to the edge. Next consider a point p on a symmetrical lifting surface which is infinitesimally close to the leading edge. The $\vec{\gamma}$-distribution everywhere except at the leading edge induces a positive vertical velocity $\partial\phi/\partial n$. At the leading edge, $\vec{\gamma}$ provides a negative vertical velocity, therefore, to satisfy $\partial\phi/\partial n = 0$ at the point p, $\vec{\gamma}$ must be infinite at the edge. A similar situation can be found in two-dimensional aerofoil theory, where there is a square root singularity at the leading edge.

There are some subtle differences in the planing problem: $\vec{\gamma}$ at the leading edge is finite and only approximately tangent to the edge. An infinite $\vec{\gamma}$ at the leading edge leads to negative infinite pressure, which violates the dynamic free surface boundary condition. Therefore $\vec{\gamma}$ at the leading edge is finite and a jet is thus formed to remove the singularity. By the formation of the jet, $\vec{\gamma}$ at the leading edge can indeed be finite, since the jet induces a negative vertical velocity at the point p. By an argument similar to that for the lifting surface, the $\vec{\gamma}$-distribution is tangent to the edge of the jet but not necessarily to the edge of the planing surface. Since the jet thickness in the chines dry area is very small, $\vec{\gamma}$ at the leading edge is almost tangent to the edge; for the chines wet section this reasoning is not true, since ε is large there.

To accurately model the vorticity properties described above, two kinds of panels are introduced. Figure 5(a) shows rectangular panel generation, which is simpler and widely used in aerodynamic modelling. Figure 5(b) shows trapezoidal panel generation. According to the expected behaviour of the vorticity, trapezoidal panels will provide better detail near the leading edge but will require more computational effort. We will discuss later how these two panel generations perform.

It is difficult to compute $\vec{\gamma}$ accurately near the leading edge by a three-dimensional panel method, even when trapezoidal panels are used. This is illustrated as follows.

At the prismatic leading edge, approximate values of γ_x and γ_y can be found by the zero-pressure condition. Assuming that $\vec{\gamma}$ is tangent to the edge even with ε (which is Tulin's[7] assumption), then

$$\gamma_x = |\vec{\gamma}| \cos\theta, \qquad \gamma_y = |\vec{\gamma}| \sin\theta. \tag{35}$$

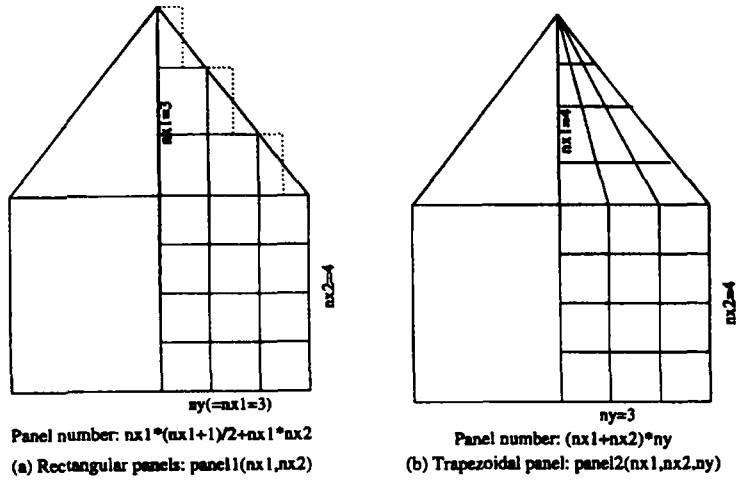

Figure 5. Two different kinds of panelization

Substituting these expressions into equation (24) yields

$$|\vec{\gamma}| = 4U \sin\theta, \tag{36}$$

$$\gamma_x = 4U \sin\theta \cos\theta, \qquad \gamma_y = 4U \sin^2\theta. \tag{37}$$

With a moderate number of panels the computed γ_x and γ_y are far less than the above desired values and $|\vec{\gamma}|$ is inaccurate. Since the purpose of the jet is to reduce $\vec{\gamma}$ to the desired value, no ε will be needed. This can be explained by considering Figures 6 and 7. These figures show the calculated transverse velocity and pressure distributions at the leading edge in addition to those from Tulin's[7] analysis. Figure 6 for a relatively small number of subpanels: $n_{x1} = n_y = 15$. It is clearly shown that even if ε does not exist, the transverse velocity at the edge is less than that of Tulin's[7] analysis; therefore the pressure is positive without the need of ε. Figure 7 is for a relatively large panel number $n_{x1} = n_y = 30$. In this case, without the existence of ε, the transverse velocity at the edge is larger than that of Tulin's[7] analysis; therefore the pressure is negative. Thus ε is introduced to make $p = 0$ at the edge. Numerical results show that for this case $\varepsilon = 0$ when $n_{x1} = n_y < 16$.

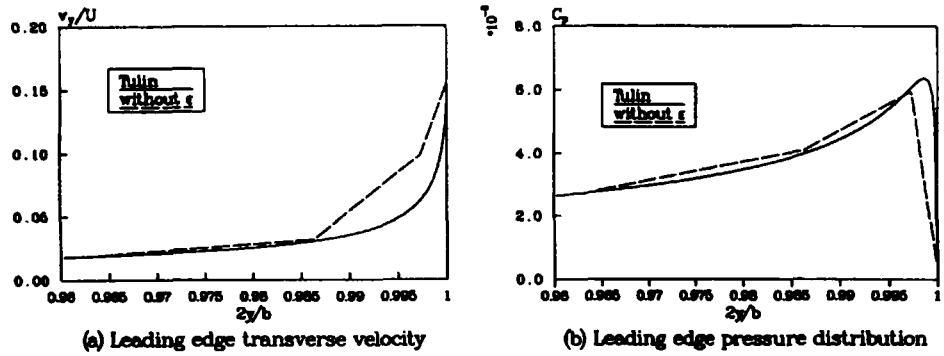

Figure 6. Leading edge transverse velocity and pressure at middle section ($x = 0{\cdot}5L_k$). $\tau = 0{\cdot}3°$ $\beta = 6°$, $\theta = 4{\cdot}55°$, $\lambda = 3{\cdot}14$. Panel 2(15,0,15): no ε is needed with coarse discretization

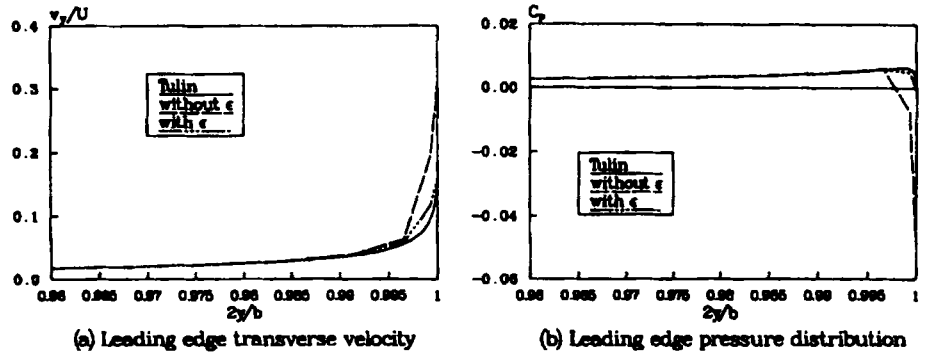

(a) Leading edge transverse velocity (b) Leading edge pressure distribution

Figure 7. Leading edge transverse velocity and pressure at middle section ($x = 0{\cdot}5L_k$). $\tau = 0{\cdot}3°$ $\beta = 6°$, $\theta = 4{\cdot}55°$, $\lambda = 3{\cdot}14$. Panel 2(30,0,30): jet is introduced with fine discretization

Cosine spacing is used since it can give very fine panels near the leading edge where the transverse velocity changes rapidly. By virtue of the singular characteristics of the vorticity distribution, the non-homogeneous panel size will not bring a convergent result when the panel number is too large and the dimension of the last panel is much smaller than the jet thickness ε. This can be observed in Figure 8(a).

Fortunately, extreme accuracy of ε in the chines dry section is not required for the transverse velocity and pressure distributions, as discussed earlier. Therefore for practical purposes an easier rectangular panelization can be used. As shown in Figure 9, the two kinds of panelization depicted in Figure 5 yield approximately equal results. The trapezoidal panelization is used to give some accurate details of a transverse section for comparison purposes. When the planing hull has a large chines wet section, the trapezoidal panel loses its advantage owing to the constrained panel size and the simpler rectangular panel will be used.

From the above comparison we conclude the following.

1. The vorticity strength and the thickness of the leading jet are difficult to calculate, but they have an insignificant influence on the calculation of the velocity and pressure distributions in the chines dry region.
2. The panelization schemes shown in Figure 5 have negligible influence on the calculation. For convenience the rectangular one is better; for higher accuracy of $\vec{\gamma}$, but not necessarily of the surface velocity and pressure at the leading edge, the trapezoidal one has the advantage.

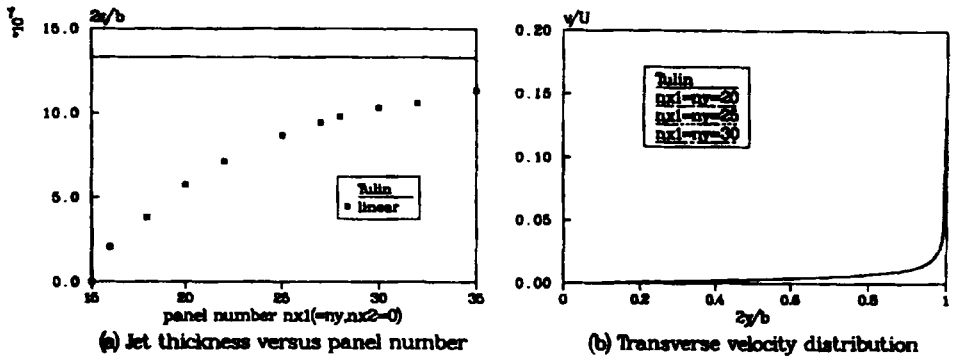

(a) Jet thickness versus panel number (b) Transverse velocity distribution

Figure 8. Numerical convergence of jet thickness ε and transverse velocity distribution at middle section ($x = 0{\cdot}5L_k$). $\beta = 6°$, $\tau = 0{\cdot}3°$, $\theta = 4{\cdot}55°$

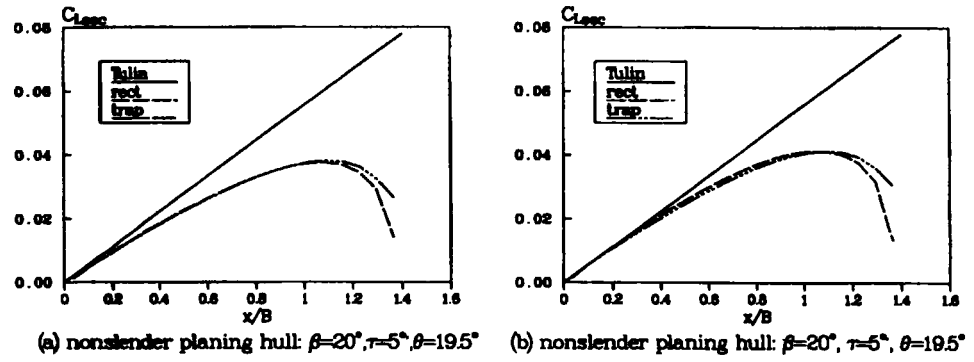

Figure 9. Sectional force comparisons for $z=0$ and $z=h$ models. Rectangular panel: panel 1(20,0). Trapezoidal panel: panel 2(20,0,20) (from Reference 13)

Condition in the jet region

There are two models in the jet: in Approach 1, as was shown in equation (25), γ_x is kept constant along a section, while in Approach 2 (i.e. Euler's equation), as was expressed in equation (31), the zero-pressure condition is satisfied in the whole jet region.

Figure 10, which shows the transverse distribution of the pressure for a chines wet section, demonstrates the difference between these two approaches. When the velocity normal to the plane is not taken into account, Approach 2 satisfies the pressure condition quite well in the whole jet region, while Approach 1 satisfies the pressure only at the leading and side edges.

Wake treatment

Since the wake is theoretically force-free, each weak panel must move with the local stream velocity, resulting in so-called 'wake roll-up'. From the steady state flow point of view the shape of the wake is not known and the process of finding the proper wake shape (wake roll-up) is achieved through iterations. As stated by Katz and Plotkin,[14] typical remedies to this problem in aerodynamics are as follows.

1. *Prescribed wake shape.* Placing the wake on the $z=0$ plane is a widely used example. A more refined alternative of this option is to prescribe the wake shape based on flow visualizations.

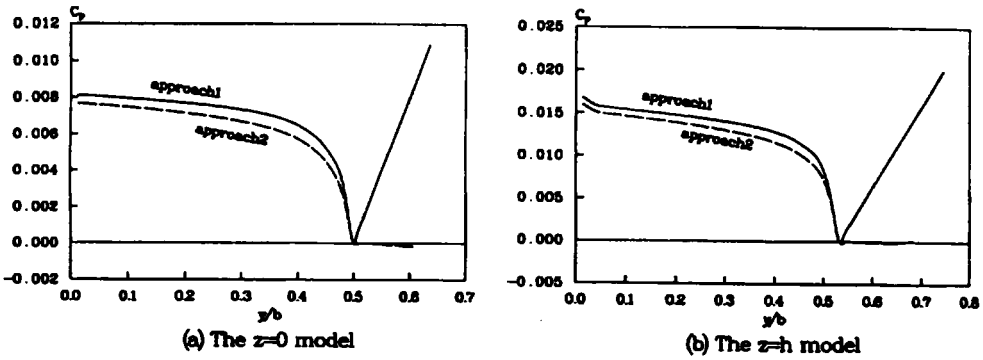

Figure 10. Pressure distribution on hull and free surface in transverse section at $x=2{\cdot}416B$, where $\lambda=2{\cdot}03$, $\lambda_k=2{\cdot}7$, $\tau=5°$, $\beta=20°$, $\theta=19{\cdot}65°$. Panel 1(20,19). Chine located at (a) $y/B=0{\cdot}5$, (b) $y/B=0{\cdot}5/\cos\beta=0{\cdot}532$

2. *Wake relaxation*. The method specifies the initial wake shape, then calculates the velocity at each of the wake points and moves the points. Iterations are continued until convergence is obtained or until sufficient wake roll-up has been achieved. This process is used by several steady state numerical solutions in aerodynamics.
3. *Time-stepping method*. This is similar to the wake relaxation method, but the time step is directly related to the motion. This time domain method can also be used for a steady state problem and requires less computational effort compared with the wake relaxation method.

In the current planing models the prescribed wake shape method is used. The other two methods may give more details about the wake but do not significantly affect the planing lift and drag. They do not only require extra computations but also have numerical uncertainties.[14] For the planing problem the roll-up process is compounded by the existence of the free surface and is thus much more complicated than in aerodynamics. Since we mainly emphasize the hydrodynamic characteristics in the hull rather than the wake, we will prescribe the wake shape.

For the $z = 0$ model the wake vorticity is also on the plane and this is analogous to the lifting line and lifting surface type of solutions. For the $z = h$ model, three different prescribed wake shapes are examined.

As is shown in Figure 11(a), the first model, which is the simplest one, extends the vortex in the direction of the planing hull, which means that the shedding vortex surface goes to infinity at an angle τ. The second model, taking into account the fact that the disturbance of the wake generally exists only at the surface, allows the wake vortex to twist its angle back to horizontal, still underneath the water surface. The third model, following the discussion in Reference 5, lets the wake vortex change its position and direction, gradually returning to the $z = 0$ plane.

Figure 11(b) shows the longitudinal force obtained by the models with these three different wake models, while all other modelling parameters remain unchanged. There is no essential difference between them, except right at the trailing edge, which is generally insignificant in the lift and moment calculation. Based upon this comparison, it is sufficiently accurate to prescribe the wake shape for the current planning problem.

Convergence of the schemes

Numerical convergence tests have been shown in Figure 8. An additional demonstration of convergence is shown in Figure 12, where the sectional lift coefficient is plotted versus different numbers of panels.

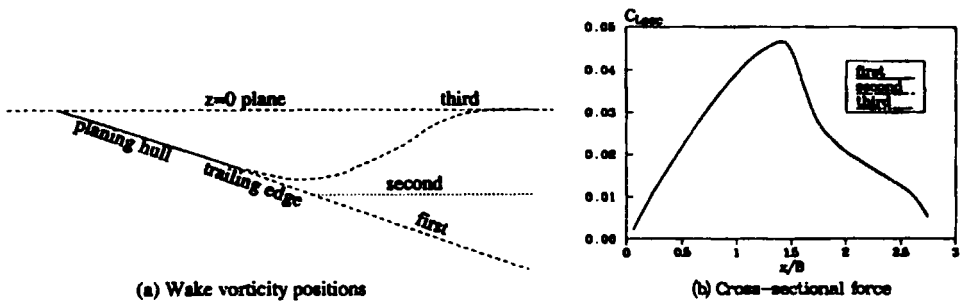

(a) Wake vorticity positions (b) Cross-sectional force

Figure 11. Wake vorticity position and its influence on lift calculation. $\beta = 20°$, $\tau = 5°$, $\theta = 18{\cdot}13°$, $\lambda = 2{\cdot}04$. Panel 1(12,10)

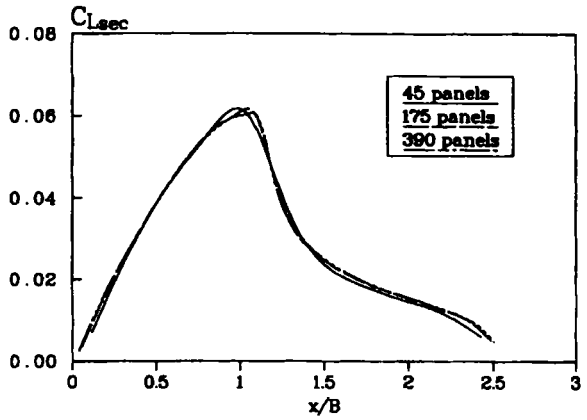

Figure 12. Convergence test for $\lambda = 2{\cdot}0$, $\tau = 5°$ $\beta = 20°$, $\theta = 23{\cdot}4°$. Panel 1(5,6) = 45, panel 1(10,12) = 175, panel (15,18) = 390

COMPARISON WITH SELECTED THEORIES AND EXPERIMENTAL DATA

Details of comparisons of the current model with selected existing theories[7,9,10] and experimental data[19,20] are given in Reference 13. In this section the comparisons are briefly summarized.

Under the slenderless assumption the current model compares well with Tulin's[7] and Vorus's[9,10] results as shown in Reference 13. The slenderness can be represented by the length/beam ratio λ or by the apex angle θ. When $\theta < 10°$, the hull can be considered as slender.

Figure 9(a) is for a non-slender hull and indicates that the rectangular and trapezoidal panels yield approximately the same result. The $z = 0$ model also compares well with Vorus's[9,10] results for a slender hull but not for a non-slender hull, as shown in Figure 13 for planing hulls with chines wet sections. For the centre and quarter-beam pressure distributions as plotted in Figure 14, the $z = h$ model yields more consistent results than the $z = 0$ model when compared with experiments. The $z = h$ model generates a lift coefficient which is consistent with Savitsky's[20] results even for a finite Froude number flow and this is shown in Figure 15.

Figure 16 shows the pressure distribution on a planing hull calculated by the $z = 0$ model. Compared with experiments, the pressure at the chines wet section is very small and this causes a loss of lift. Figure 17 shows the pressure distribution for the same planing hull but for the $z = h$ model. Compared

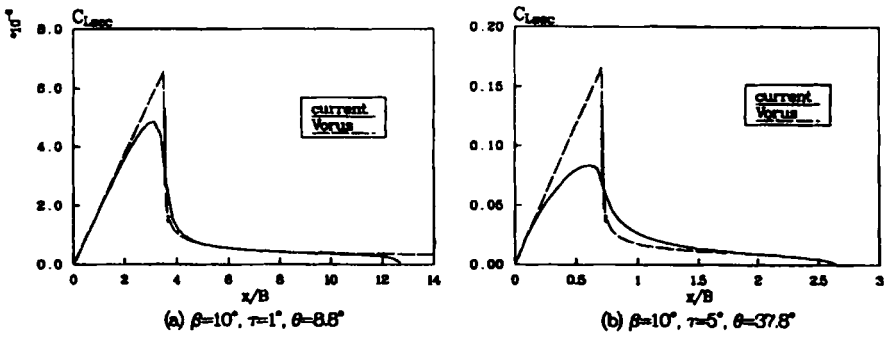

Figure 13. Planing hull with chines wet part; longitudinal force compared with Vorus's[9,10] non-linear results. (a) Slender: panel 1(15,40). (b) Non-slender: panel 1(12,34) (from Reference 13)

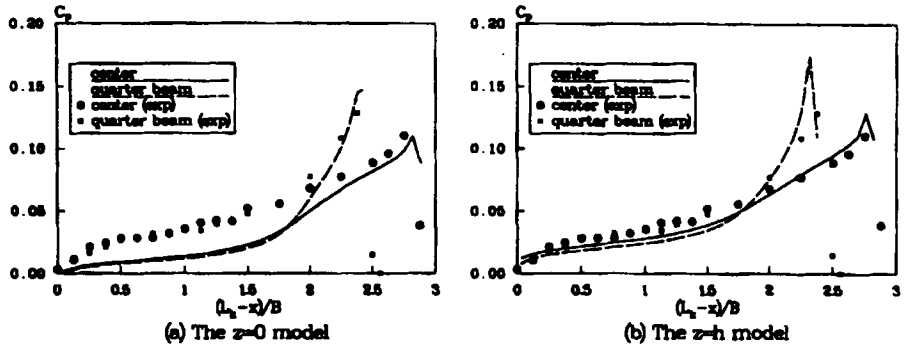

Figure 14. Centre and quarter-beam pressure distribution calculated for large λ, compared with Kapryan and Boyd's[19] experimental data. $\tau = 6°$ $\beta = 20°$, $\lambda = 2{\cdot}4$, $\theta = 27{\cdot}7°$. Panel 1(10,37) for both (from Reference 13)

with the $z = 0$ model, the maximum pressure in the chines dry area is approximately 45% higher. The effect of the reduced pressures is reflected in a lower lift coefficient: $C_L = 0{\cdot}060$ for the $z = 0$ model and $C_L = 0{\cdot}080$ for the $z = h$ model. For reference the experimental lift coefficient from Savitsky's[20] work is $C_L = 0{\cdot}077$. In Figure 17 there is also a local pressure maximum along the keel area. This increased pressure has not been observed in existing experimental results, which generally lack the spatial resolution necessary to define the slight changes. However, Vorus[10] has identified similar behaviour for impacting cylinders with large dead-rise angles.

CONCLUSIONS

This paper focuses on numerical details of a suitable vortex lattice method for a three-dimensional planing hull model. The existence of the free surface represents the major difference and source of difficulty for the planing problem when compared with the aerodynamic wing problem. Instead of a vortex roll-up model similar to those used in the study of the separation of a delta wing, a special vortex condition is applied to obtain accurate details at the leading and side edges, thus satisfying the

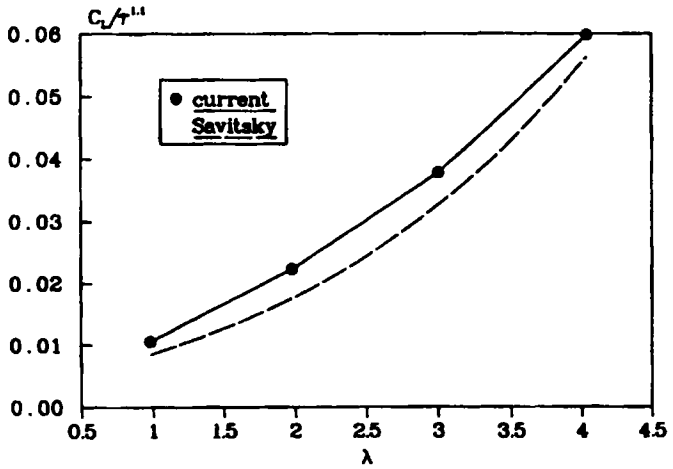

Figure 15. Influence of gravity: $F_n = 2$. Lift coefficient versus λ. $\beta = 20°$ $\tau = 5°$. Panel numbers: panel 1(31,7) for $\lambda = 1{\cdot}01$, panel 1(21,19) for $\lambda = 1{\cdot}97$, panel 1(19,31) for $\lambda = 2{\cdot}99$, panel 1(15,35) for $\lambda = 4{\cdot}04$ (from Reference 13)

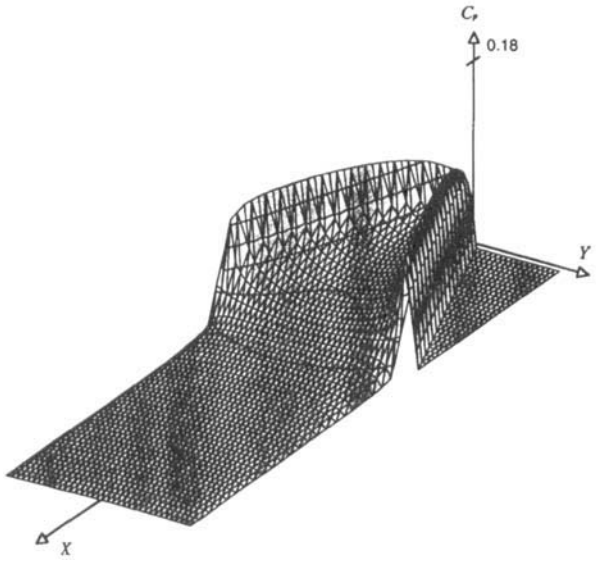

Figure 16. Pressure distribution on entire body surface, calculated by $z=0$ model. $\beta=20°$, $\tau=5°$, $\lambda=2{\cdot}5$. Panel number: panel 1(18,24)

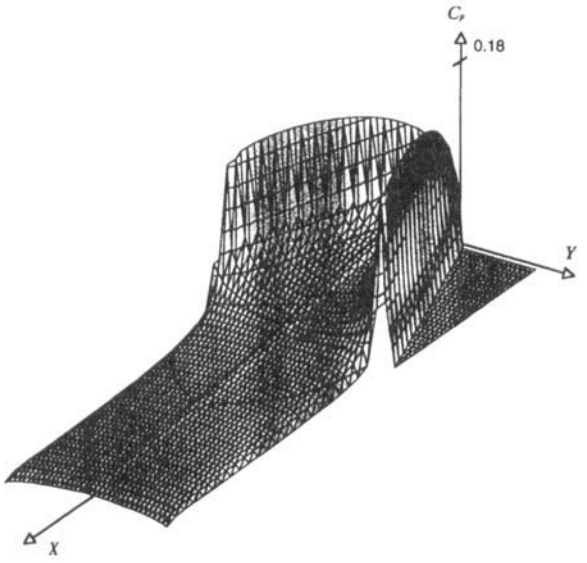

Figure 17. Pressure distribution on entire body surface, calculated by $z=h$ model. $\beta=20°$, $\tau=5°$, $\lambda=2{\cdot}5$. Panel number: panel 1(18,24)

zero-pressure condition. For a hull with a chines wet section a new scheme satisfying the Euler equation is implemented for the zero-pressure condition.

It is demonstrated that the model presented by this paper yields sufficiently consistent results when compared with experiments, even for a finite Froude number flow where gravity effects are introduced locally. Further study should be directed towards exploring the details of flow characteristics such as the wetted surface, the precise wake location, the jet spray and the wave generation, all of which are simplified here.

ACKNOWLEDGEMENTS

This work was supported by the Michigan Sea Grant College Program, projects R/T-31 and R/T-32, under grant number NA89AA-D-SG083 Amd#5 from the Office of Sea Grant, National Oceanic and Atmospheric Administration (NOAA), U.S. Department of Commerce and funds from the State of Michigan.

The authors would like to thank Professor W. Vorus for his kind help, including long technical discussions and access to his wedge impact software.

REFERENCES

1. L. Prandtl, 'Applications of modern hydrodynamics to aeronautics', *NCAA TR 116*, 1922.
2. R. Lagendre, 'Vortex sheets rolling-up along leading-edge of delta wings', *Prog. Aero. Sci.*, **VII**, 7–33 (1966).
3. H. W. M. Hoeijmakers, 'Computational vortex flow aerodynamics', *AGARD Conf. Proc.*, **342**, (1983).
4. C. P. Mracek and D. T. Mook, 'Numerical simulation of three-dimensional lifting flows by a vortex panel method', *Proc. AIAA Atmospheres Flight Mechanics Conf.*, Minneapolis, MN, August 1988, AIAA, New York, 198X.
5. H. Wagner, Über Stoss- und Gleitvorgänge an der Oberflächen von Flüssigkeiten, *Z. Angew. Math. Mech.*, **12**, 193–215 (1932).
6. A. E. Green, 'Note of sliding of a plate on the surface of a stream', *Proc. Camb. Philos. Soc.*, **32**, 248–252 (1936).
7. M. P. Tulin, 'The theory of slender surfaces planing at high speed', *Schiffstecknik*, **4**, 125–133 (1956).
8. R. Zhao and O., Faltinsen, 'Water entry of two-dimensional bodies', *Proc. Seventh Int. Workshop on Water Waves and Floating Bodies*, Val de Reuil, May 1992.
9. W. S. Vorus, 'An extended slender body model for planing hull hydrodynamics;, presented at *SNAME Great Lakes and Great Rivers Section Meet.*, Cleveland, OH January 1992.
10. W. S. Vorus, 'A Flat cylinder Theory for Vessel Impact and Steady Planing Resistance', *J. Ship Research*, in press (1996).
11. T. F. Ogilvie, 'Instabilityof planing surfaces', *Department of Naval Architecture and Marine Engineering, Rep. 026*, University of Michigan, Ann Arbor, MI, 1971.
12. T. F. Ogilvie and Y. T. Shen, 'Flutter-like oscillations of a planing plate', *Department of Naval Architecture and Marine Engineering, Rep. 146*, University of Michigan, Ann Arbor, MI, 1973.
13. C. Lai and A. W. Troesch, 'Modeling issues related to the hydrodynamics of three dimensional steady planing', *J. Ship Res.*, **39**, 1–24 (1995).
14. J. Katz and A. Plotkin, *Low-Speed Aerodynamics*, McGraw-Hill, New York, 1991.
15. T. Brockett, *NAME520 Lecture Notes*, Department of Naval Architecture and Marine Engineering, University of Michigan, Ann Arbor, MI, 1987.
16. D. T. Mook, 'A computer-based method for analyzing the flow over sails', *Proc. Fourth Chesapeake Sailing Yacht Symp.*, 1979.
17. D. F. Thrasher, 'Application of the vortex-lattice concept to flows with smooth-surface separation', *Proc. Fourteenth Symp. on Naval Hydrodynamics*, 1983, pp. 1089–1113.
18. C. Lai, 'Three-dimensional planing hydrodynamics based on a vortex lattice method', *Ph.D. Thesis*, University of Michigan, Ann Arbor, MI 1994.
19. W. J. Kapryan and G. M. Boyd Jr., 'Hydrodynamic pressure distributions obtained during a planing investigation of five prismatic surfaces', *National Advisory Committee for Aeronautics, Tech. Note 3477*, 1955.
20. D. Savitsky, 'Hydrodynamics design of planing hulls', *Marine Technology.*, **1**, (1964).